Available online at www.sciencedirect.com
SCIENCE DIRECT®
Inorganica Chimica Acta 350 (2003) 299–313
Inorganica Chimica Acta
www.elsevier.com/locate/ica

Use of the cationic fragments $[Ru(\eta^5\text{-}C_5H_5)(MeCN)_3]^+$ and $[M(\eta^6\text{-}C_6H_5R)(MeCN)_3]^+$ (M = Os, Ru; R = H, Me) as ionic coupling reagents with the anions $[H_2Os_4(CO)_{12}]^{2-}$, $[Os_4(CO)_{13}X]^-$ (X = Cl, Br, I) and $[Os_4(CO)_{13}]^{2-}$ in the synthesis of arene and cyclopentadienyl clusters

Muna R.A. Al-Mandhary [a], Radchada Buntem [a], Christopher Cathey [a], Jack Lewis [a], M. Carmen Ramirez de Arellano [a], Gregory P. Shields [a], Cheryl L. Doherty [b], Paul R. Raithby [b,*]

[a] *Department of Chemistry, Lensfield Road, Cambridge CB2 1EW, UK*
[b] *Department of Chemistry, University of Bath, Claverton Down, Bath BA2 7AY, UK*

Received 28 June 2002; accepted 23 September 2002

This paper is dedicated to Professor Pierre Braunstein in recognition of his outstanding contribution to organometallic and cluster chemistry.

Abstract

The cluster $[H_2Os_4(CO)_{13}]$ may be reduced with K/Ph_2CO to generate an anion which reacts with $[M(\eta^6\text{-}C_6H_5R)(MeCN)_3]^{2+}$ (M = Os, Ru; R = H, Me) affording the capped clusters $[H_2Os_4M(CO)_{12}(\eta^6\text{-}C_6H_5R)]$ (M = Os, R = H (**1**); M = Ru, R = H (**2**); M = Os, R = Me (**3**)) with the arene ligand on one of the axial site of a trigonal bipyramid. The Os clusters **1** and **3** transform into the more stable equatorial isomers, **4** and **5**, respectively, in 24 h. The structure of **5** has been confirmed by a single crystal X-ray diffraction study, and all the complexes have been characterised spectroscopically. The axial isomers may be carbonylated or hydrogenated to generate the edge-bridged tetrahedral clusters $[H_2Os_4M(CO)_{13}(\eta^6\text{-}C_6H_5R)]$ (M = Os, R = H (**6**); M = Ru, R = H (**7**); M = Os, R = Me (**8**)) and the known clusters $[H_4Os_4M(CO)_{12}(\eta^6\text{-}C_6H_6)]$ (M = Os (**9**); Ru (**10**)). The structure of **7** has been confirmed by an X-ray diffraction analysis. The axial isomer **1** reacts with PPh_2Me to yield the addition product $[H_2Os_5(CO)_{12}(\eta^6\text{-}C_6H_6)PPh_2Me]$ (**11**), whereas the mixed osmium–ruthenium analogue undergoes a transformation to the 'spiked' tetrahedral $[H_3Os_4Ru(CO)_{12}(\mu_3\text{-}\sigma,\sigma,\eta^6\text{-}C_6H_5)PPh_2Me]$ (**12**). Deprotonation of the axial isomers **1** and **2** and subsequent reaction with $[AuPPh_3]^+$ yields $[HOs_4M(CO)_{12}(C_6H_6)(AuPPh_3)]$ (M = Os (**13**); Ru (**14**)). As well as spectroscopic characterisation cluster, the structures of **11**, **12** and **13** have been established by X-ray diffraction experiments. In a related series of reactions the cluster monoanion $[Os_4(CO)_{13}X]^-$ (X = Cl (**15**), Br (**16**), I (**17**)) may be capped using the monocation $[Ru(\eta^5\text{-}C_5H_5)(MeCN)_3]^+$ affording $[HOs_4Ru(CO)_{13}(\eta^5\text{-}C_5H_5)]$ (**18**), which is readily deprotonated and further capped with $[AuPPh_3]^+$ to afford the neutral cluster $[Os_4(CO)_{13}Ru(\eta^5\text{-}C_5H_5)AuPPh_3]$ (**20**). The structures of **15**, **18** and **20** have been established crystallographically. The cluster anion $[Os_4(CO)_{13}X]^-$ may be reduced with K/Ph_2CO and the resulting anionic complex coupled with $[Ru(\eta^5\text{-}C_5H_5)(MeCN)_3]^+$, providing another route to $[Os_4Ru(CO)_{13}(\eta^5\text{-}C_5H_5)]^-$ (**19**). This anionic complex may also be coupled with $[Ru(\eta^6\text{-}C_6H_6)(MeCN)_3]^{2+}$ affording $[Os_4Ru(CO)_{13}(\eta^6\text{-}C_6H_6)]$ (**21**) which has also been structurally characterised.

Keywords: Cluster; Carbonyl; Osmium; Ruthenium; Gold; Arene; Cyclopentadiene; Crystal structures

1. Introduction

Use of mono- and dicationic capping reagents in cluster build-up reactions is now a well-established synthetic technique for the production of both homo-

* Corresponding author. Tel.: +44-1225-323 183; fax: +44-1225-826 231.
E-mail address: p.r.raithby@bath.ac.uk (P.R. Raithby).

0020-1693/03/$ - see front matter © 2003 Elsevier Science B.V. All rights reserved.
doi:10.1016/S0020-1693(02)01516-5

metallic and mixed-metal species [1]. In Ru and Os cluster chemistry, initial investigations focused on the dicationic species '$M(C_6H_5R)^{2+}$' (M = Os, Ru; R = H, Me) with the anions $[Os_3(CO)_9(R^1C_2R^2)]^{2-}$ ($R^1 = R^2 =$ Me, Et, Ph; R^1 = Me, R^2 = H, Et, Ph) [2], $[Os_4H_4(CO)_{11}]^{2-}$ [3,4], $[Os_5(CO)_{15}]^{2-}$, $[Os_6(CO)_{17}]^{2-}$ and $[Os_7(CO)_{20}]^{2-}$ [5].

Monocationic species, when allowed to react with dianions, offer the possibility of increasing cluster nuclearity by two metal atoms in one step, with the additional advantage of lower redox activity. Both mono- and bicapped species have been produced successfully via the reaction of $[Ru(\eta^5\text{-}C_5H_5)(MeCN)_3]^+$ with a wide range of dianions, including $[Os_5(CO)_{15}]^{2-}$ [6], $[Ru_5C(CO)_{14}]^{2-}$, $[Ru_6C(CO)_{16}]^{2-}$ [7], $[Os_3(CO)_{11}]^{2-}$ [8], and more recently mixed Os–Co [9], Os–Au [10], and phosphine-substituted species [11].

The structures of many of the penta-, hexa- and heptanuclear species have been summarised in a recent review [12]. We have previously published a preliminary report on the product of the reaction of '$[H_2Os_4(CO)_{12}]^{2-}$' with '$Ru(C_6H_6)^{2+}$' followed by the addition of $P(OMe)_3$ to form a spiked tetrahedral cluster with an orthometallated arene ring [13]. In this paper, we describe further the reactions of '$[H_2Os_4(CO)_{12}]^{2-}$' and extend them to the related tetranuclear anions $[Os_4(CO)_{13}X]^-$ (X = Cl, Br, I) and '$[Os_4(CO)_{13}]^{2-}$', and compare the reactivity of the capped products formed.

2. Results and discussion

2.1. Reaction of $[H_2Os_4(CO)_{12}]^{2-}$ with $[M(\eta^6\text{-}C_6H_5R)]^{2+}$ (R = H, Me)

The neutral cluster $[H_2Os_4(CO)_{13}]$ was reduced with potassium benzophenone ketyl in THF and the resulting dianion reacted readily with the cationic reagents $[M(\eta^6\text{-}C_6H_6)(MeCN)_3][BF_4]_2$ (M = Os, Ru) and $[Os(\eta^6\text{-}C_6H_5Me)(CF_3SO_3)_2]$ to produce the clusters $[H_2Os_5(CO)_{12}(C_6H_6)]$ (**1**), $[H_2Os_4Ru(CO)_{12}(C_6H_6)]$ (**2**) and $[H_2Os_5(CO)_{12}(C_6H_5Me)]$ (**3**) (Scheme 1). The electron count of 72 electrons is consistent with these complexes having a trigonal bipyramidal metal framework. These products were unstable both in solution and in the solid state, and must be purified, characterised or reacted further within minutes of preparation. However, it was possible to obtain IR, ^1H NMR and mass spectra for these species (Table 1). The IR spectra for the three complexes are very similar which suggests that **1**–**3** are structurally analogous. Cluster **2** shows a broad resonance at δ −13.75 in the ^1H NMR spectrum but no such hydride peak was observed for **1** or **3** at room temperature; the arene-H resonance is consistent with the η^6 bonding mode in each case.

On standing for 24 h in dichloromethane solution, **1** and **3** each undergo a colour change, and in each case two new products **4** and **6** and **5** and **8**, respectively, were isolated from the resulting mixture in approximately equal (~40%) yield. Products **4** and **5** have very similar IR spectra and the spectroscopic and mass spectrometric data (Table 1) suggests that **4** and **5** are isomers of **1** and **3** with the same trigonal bipyramidal metal framework but with the arene ligand coordinated in a different position. Electronic considerations indicate that the greater donor character of the metal-arene $M(\eta^6\text{-arene})$, or a $M(\eta^5\text{-}C_5H_5)$ fragment, compared with a metal-tricarbonyl unit, enhances electron density donation from the formally $20e^-$ (equatorial) to the $17e^-$ (axial) sites, stabilising the trigonal bipyramidal cluster, and hence, where steric constraints permit, the $M(\eta^6\text{-}C_6H_6)$ group should occupy the 'electron-rich' centre in the more stable isomer [12]. Unlike **1**, **2** and **3**, **4** and **5** are both thermodynamically stable and **5** was crystallised by slow diffusion from benzene solution and the solid state structure determined by single-crystal X-ray diffraction (Table 2). Consistent with the spectroscopic evidence, the cluster **5** does has a trigonal bipyramidal Os_5 core with the toluene ligand coordinated to the equatorial Os(5) as shown in Fig. 1. The hydride ligands where not located, but potential energy calculations [14] suggest that they bridge the Os(2)–Os(3) and Os(2)–Os(4) edges. The structure is similar to those of the tetrahydrido clusters $[H_4Os_4M(CO)_{11}(\eta^6\text{-}C_6H_6)]$ (M = Os, Ru) prepared by reducing $[Os_4H_4(CO)_{12}]$ with potassium diphenylketyl and reacting the resulting anion with $[M(\eta^6\text{-}C_6H_6)(MeCN)_3]$ (M = Ru, Os) [4]. The $[H_4Os_4M(CO)_{11}(\eta^6\text{-}C_6H_6)]$ clusters, which are the initial products of the reaction have arene ligand in the equatorial site and are thermodynamically stable.

2.2. Reaction of 1–3 with carbon monoxide

In addition to **4** and **5**, **1** and **3** also yield carbonyl-scavenging products $[H_2Os_5(CO)_{13}(C_6H_5R)]$ (R = H (**6**), R = Me (**8**)) (Scheme 1). On standing, **2** does not yield any isomerisation product, but also produces the carbonylated product $[H_2Os_4Ru(CO)_{13}(C_6H_6)]$ (**7**) in approximately 15% yield along with decomposition products. Clusters **6**–**8** may also be synthesised directly by bubbling CO through dichloromethane solutions of **1**–**3**, respectively, for 30 min. For **1** and **2**, the addition is quantitative, but for **3** approximately 30% of the isomerisation product **5** is also obtained. The addition of CO to **1** and **2** is irreversible, no change being observed when **6** and **7** are heated under reflux in toluene for 1 h.

The IR spectra of **6**–**8** are very similar, suggesting that the structures are analogous, and the ^1H NMR and

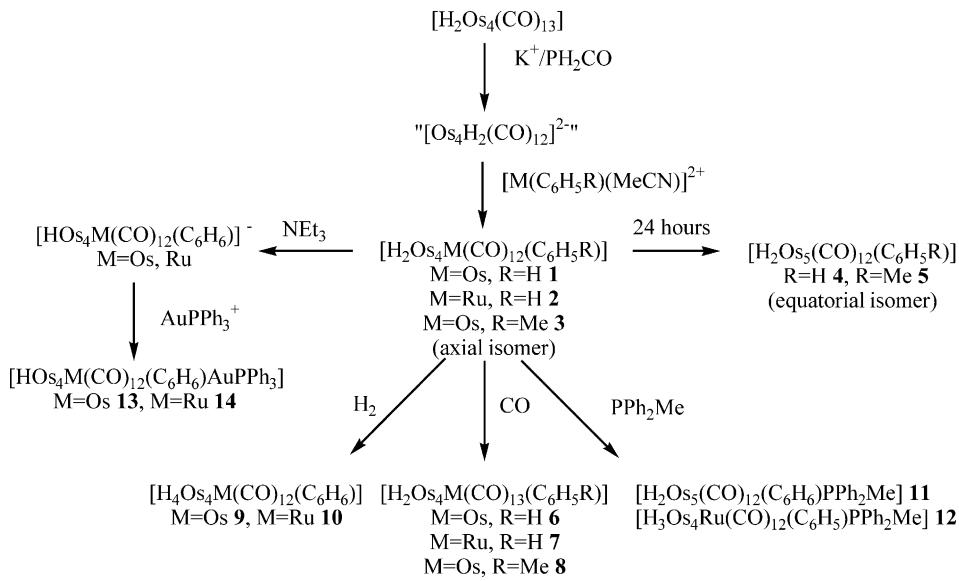

Scheme 1.

mass spectra are consistent with the proposed formulae. The addition of CO to a trigonal bipyramidal Os_4Ru core results in an increase in the electron count of two electrons, and 74 electron systems usually exhibit a square-based pyramidal or edge-bridged tetrahedral core. The latter would be expected by analogy with the related dihydrido clusters $[H_2Os_5(CO)_{16}]$ [15] and $[H_2Os_4Rh(CO)_{13}(\eta^5\text{-}C_5R_5)]$ (R = H, Me) [16,17]. $[H_2Os_4Ru(CO)_{13}(\eta^6\text{-}C_6H_6)]$ (**7**) was crystallised by slow diffusion of hexane into a saturated dichloromethane solution and a single-crystal X-ray analysis confirmed the edge-bridge tetrahedral molecular structure. The molecular structure is shown in Fig. 2 and selected bond parameters are listed in Table 3. The hydride ligands were not located, but potential energy calculations [14] suggest that they bridge the two longest edges, Os(1)–Os(3) and Os(2)–Os(3) as in the $[H_2Os_4Rh(CO)_{13}(\eta^5\text{-}C_5R_5)]$ [12] analogues, while the shortest Os(1)–Os(2) edge is bridged by the Ru(1) atom. The bond parameters for **7** are also very similar to those in $[H_2Os_4Rh(CO)_{13}(\eta^5\text{-}C_5R_5)]$ (R = H, Me) [12].

2.3. Reaction of *1* and *2* with dihydrogen

On bubbling H_2 through dichloromethane solutions of **1** and **2** a gradual colour change from purple and maroon, respectively, to green occurs over a period of 2 h (Scheme 1). The resulting clusters **9** and **10** were produced in near quantitative yield. The IR spectra of **9** corresponds to that for the previously reported compound $[H_4Os_5(CO)_{12}(\eta^6\text{-}C_6H_6)]$ (**9**) [4] and that of **10** is very similar, suggesting the corresponding formulation $[H_4Os_4Ru(CO)_{12}(\eta^6\text{-}C_6H_6)]$ (**10**).

2.4. Reaction of *1* and *2* with PPh_2Me

Clusters **1** and **2** react rapidly with PPh_2Me in dichloromethane at room temperature to yield a dull green–brown product $[H_2Os_5(CO)_{12}(PPh_2Me)(\eta^6\text{-}C_6H_6)]$ (**11**) and bright orange compound $[H_3Os_4\text{-}Ru(CO)_{12}(\mu_3\text{-}\sigma,\sigma,\eta^6\text{-}C_6H_5)PPh_2Me]$ (**12**), respectively (Scheme 1). These products are not structurally analogous, unlike those from the addition reactions with CO and H_2, as demonstrated by their IR, ^1H and ^{31}P NMR spectra (Table 1). Cluster **11** shows a singlet η^6-benzene resonance and two hydride resonances, one of which exhibits coupling with the ^{31}P of the phosphine (J_{PH} = 14.4 Hz). These data are consistent with a simple addition reaction of phosphine, which is confirmed by a diffraction study of a single crystal grown by slow evaporation from benzene. The molecular structure of **11** is shown in Fig. 3 and selected bond parameters are presented in Table 4. The cluster has an edge-bridged tetrahedral geometry, the phosphine addition having occurred at an equatorial site with the 'Os(CO)(η^6-C_6H_6)' unit adopting the edge-bridging position. The hydride ligands were not located, but potential energy calculations indicate that they bridge the Os(2)–Os(5) and Os(3)–Os(5) edges, as in $[H_2Os_5(CO)_{16}]$, consistent with the observed J_{PH} coupling. The structure is closely related to that of **7**, PPh_2Me replacing one of the CO ligands. This causes a distortion of the ligand polyhedron, and combined with electronic effects results in an incipient CO bridge between C(12) and the edge-bridging Os(1) centre [Os(1)–C(12) 2.57(5) Å, Os(2)–C(12)–O(12) 162(4)°]; the *cis* edge Os(3)–Os(1) is considerably longer [2.878(2) Å] than the edge with the incipient bridge [2.801(2) Å].

Table 1
Spectroscopic data for the new complexes

	IR, ν(CO) (cm^{-1}) [a]	Mass (m/z) exptl. (calc.)	^{1}H NMR δ; J (Hz) [d]	^{13}C NMR δ [d]	^{31}P NMR
1	2082(m), 2038(vs), 2028(s), 1995(w), 1981(w)	1367(1366) [f]	6.16 (s, 6H, C_6H_6)		
2	2081(m), 2038(vs), 2028(s), 1997(w), 1981(w)	1280 (1277) [f]	5.99 (s, 6H, C_6H_6), −13.75 (s br, 2H, Os–*H*–Os)		
3	2081(m), 2036(vs), 2026(s), 1993(w), 1977(w)		6.25–5.92 (m, 5H, C_6H_5Me), 2.40 (s, 3H, C*H*$_3$)		
4	2079(w), 2055(vs), 2037(w), 2019(m), 2001(vs), 1969(w), 1921(w), 1785(wbr)	1367 (1366) [f]	6.16 (s br, 6H, C_6H_6)		
5	2078(w), 2055(vs), 2035(w), 2018(m), 2000(vs), 1967(m), 1920(w), 1794(wbr)	1382 (1380) [f]	6.58–5.94 (m, 5H, C_6H_5Me), 2.51 (s, 3H, C*H*$_3$), −12.35 (s br, 2H, Os–*H*–Os), −20.96 (s, 2H, Os–*H*–Os)		
6	2083(m), 2048(s), 2029(vs), 1995(m), 1985(m), 1956(w)	1396 (1394) [f]	6.04 (s, 6H, C_6H_6), −19.50 (s, 2H, Os–*H*–Os)		
7	2083(w), 2049(m), 2028(vs), 1998(m), 1986(m), 1935(w)	1308 (1305) [f]	6.09 (s, 6H, C_6H_6), −18.66 (s, 2H, Os–*H*–Os)		
8	2082(w), 2048(m), 2028(vs), 1996(w), 1984(w), 1939(w)	1408 (1408) [f]	6.30–5.69 (m, 5H, C_6H_5Me), 2.51 (s, 3H, C*H*$_3$), −19.52 (s br, 2H, Os–*H*–Os)		
11	2074(s), 2039(vs), 2018(s), 1996(s), 1975(m), 1942(w)	1569 (1566)	7.6 (m, 10H, Ph), 5.42 (s, 6H, C_6H_6), 2.64(d, 3H, Me, $J_{PH} = 9.8$ Hz) −17.65 (dd, 1H, Os–*H*–Os, $J = 1.8$, $J_{PH} = 14.4$ Hz), −19.27 (s, 1H, Os–*H*–Os)		−167.07 (s, 1P)
12	2079(m), 2052(s), 2029(vs), 2012(s), 1971(m)	1481 (1479) [f]	7.5 (m, 10H, Ph), 6.51 (t, CH, $J = 5$), 5.31 (t, CH, $J = 6$), 4.86 (m, CH), 4.05 (d, CH, $J = 6.9$) 3.99 (d, CH, $J = 7.5$), 2.02 (d, 3H, $J_{PH} = 9.2$), −8.71 (1H, $J_{PH} = 19.5$), −20.98 (s, 1H) −21.63 (s, 1H).		−106.98 (s, 1P)
13	2057(w), 2029(vs), 2015(s), 1994(m), 1977(m), 1953(m)	1824 (1479) [f]	7.4 (m, 15H, Ph), 5.90 (s, 6H, C_6H_6), −12.11 (s, 1H, Os–*H*–Os)		
14	2057(w), 2030(vs), 2015(s), 1993(m), 1977(m), 1954(m)	1738 (1736) [f]	7.4 (m, 15H, Ph), 5.80 (s, 6H, C_6H_6), −12.11 (s, 1H, Os–*H*–Os)		
15	2069(w), 2034(s), 2012(s), 1971(m), 1805(wbr).	1160 [e] (1160.3)			
16	2069(w), 2032(s), 2013(s), 1971(m), 1801(wbr).	1205 [e] (1204.7)			
17	2068(w), 2030(s), 2012(s), 1968(m), 1801(wbr)	1251 [e] (1251.7)			
18	2087(w), 2057(vs), 2029(ssh), 2019(s), 2002(msh), 1977(wbr), 1928(wbr), 1722(wbr)	1298 [b] (1300)	−17.50 (s, 1H, Os–H–Os) 5.47 (s, 5H, C_5H_5)	82.75 (s, 5C, C_5H_5)	
19	2050(w), 2016(s), 1991(m), 1978(m), 1942(mvbr), 1722(wbr)	1297 [c] (1299)	5.3 (s, 5H, C_5H_5)		
20	2065(w), 2036(vs), 2017(s), 2005(s), 1981(mbr), 1932(mvbr)	1760 [b], 1758 [c] (1760)	5.42 (s, 5H, C_5H_5) 7.51 (m, 15H, Ph)	85.45 (s, 5C, C_5H_5) 130.69 (m, 18C, Ph)	77.02 (s, 1P, AuP)
21	2075(w), 2045(s), 2020(msh), 2010(m), 1978(wbr), 1924(vwbr)	1314 [c] (1312)	6.49 (s, 6H, C_6H_6)		

v, very; s, strong; m, medium; w, weak; sh, sharp; and br, broad.
[a] Spectra run in CH_2Cl_2.
[b] Positive-ion FAB based on ^{102}Ru and ^{192}Os.
[c] Negative-ion FAB based on ^{102}Ru and ^{192}Os.
[d] Spectra run in $CDCl_3$.
[e] Negative-ion FAB.
[f] Positive-ion FAB based on ^{101}Ru and ^{190}Os.

Table 2
Selected bond lengths (Å) and angles (°) for **5**

Os(1)–Os(2)	2.792(3)	Os(1)–Os(3)	2.832(3)
Os(1)–Os(4)	2.803(3)	Os(1)–Os(5)	2.827(3)
Os(2)–Os(3)	2.767(3)	Os(2)–Os(4)	2.778(3)
Os(2)–Os(5)	2.815(3)	Os(3)–Os(5)	2.797(3)
Os(4)–Os(5)	2.810(4)	Os(1)–C(1)	2.47(6)
Os(5)–C(1)	1.87(6)	Os(5)–C(C_6H_5Me)	2.22(6)–2.38(6)
Os(1)–C(1)–Os(5)	80(2)	Os(1)–C(1)–O(1)	119(5)
Os(5)–C(1)–O(1)	158(5)		

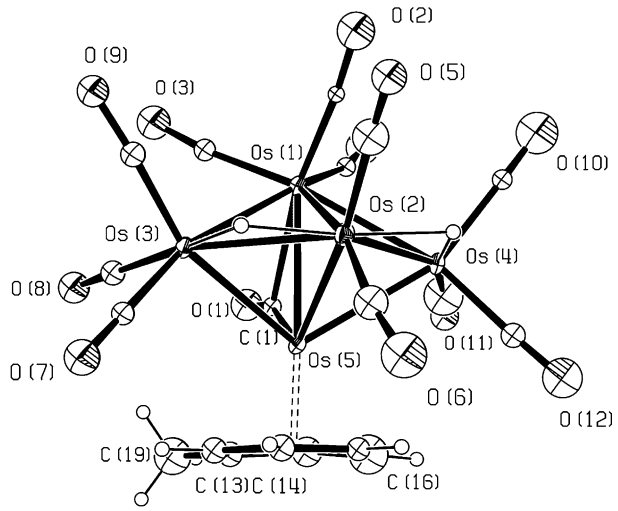

Fig. 1. The molecular structure of [$H_2Os_5(CO)_{12}(\eta^6$-C_6H_5Me)] (**5**); the ellipsoids are shown at the 30% probability level.

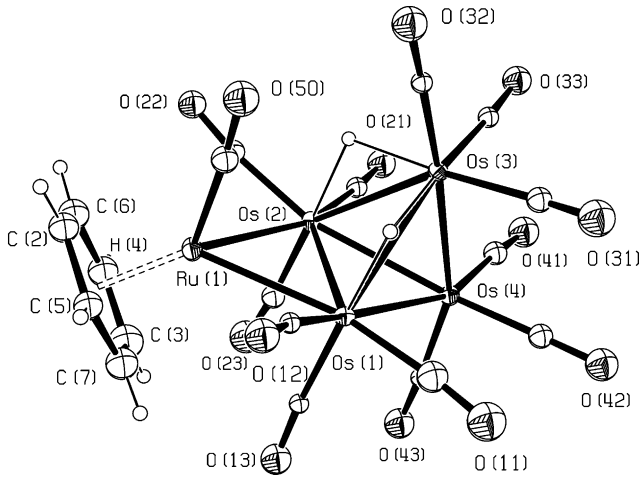

Fig. 2. The molecular structure of [$H_2Os_4Ru(CO)_{13}(\eta^6$-$C_6H_6$)] (**7**); the ellipsoids are shown at the 30% probability level.

Conversely, **12** displays three hydride resonances in the ^{1}H NMR spectrum in a 1:1:1 ratio, a doublet (J_{PH} = 19.5 Hz) and two singlets. The arene region of the spectrum is considerably more complex than that of **11**, with five resonances with the same integration, suggesting that a proton has been transferred from the arene

Table 3
Selected bond lengths (Å) and angles (°) for **7**

Os(1)–Os(2)	2.7527(16)	Os(1)–Os(3)	2.9622(16)
Os(1)–Os(4)	2.8216(17)	Os(1)–Ru(1)	2.829(3)
Os(2)–Os(3)	2.9592(17)	Os(2)–Os(4)	2.8339(17)
Os(2)–Ru(1)	2.842(3)	Os(3)–Os(4)	2.7791(18)
Ru(1)–C(C_6H_6)	2.23(4)–2.28(4)		
Os(1)–Ru(1)–Os(2)	58.07(5)	Ru(1)–Os(1)–Os(3)	98.85(6)
Ru(1)–Os(2)–Os(3)	98.63(7)		

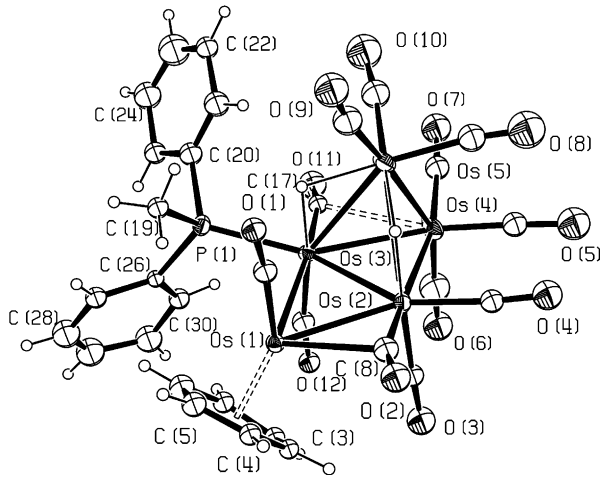

Fig. 3. The molecular structure of [$H_2Os_5(CO)_{12}(\eta^6$-C_6H_6)PPh_2Me] (**11**); the ellipsoids are shown at the 30% probability level.

Table 4
Selected bond lengths (Å) and angles (°) for **11**

Os(1)–Os(2)	2.8035(18)	Os(1)–Os(3)	2.879(2)
Os(2)–Os(3)	2.775(2)	Os(2)–Os(4)	2.791(2)
Os(2)–Os(5)	2.957(2)	Os(3)–Os(4)	2.847(2)
Os(3)–Os(5)	2.972(2)	Os(4)–Os(5)	2.796(2)
Os(1)–C(C_6H_6)	2.20(3)–2.34(4)	Os(3)–P(1)	2.394(9)
Os(2)–C(8)	1.94(4)	Os(1)–C(8)	2.56(4)
Os(1)–Os(3)–P(1)	88.6(2)	Os(2)–Os(3)–P(1)	144.2(3)
Os(4)–Os(3)–P(1)	151.1(2)	Os(2)–C(8)–O(2)	160(3)
Os(1)–C(8)–O(2)	124(3)		

ring to the metal core. The ^{1}H NMR and IR spectra are similar to those for the previously reported cluster [$H_3Os_4(CO)_{12}Ru\{P(OMe)_3\}(\eta^6$-$C_6H_5$)] [13] which was prepared by a similar route. In that case, another product [$H_2Os_4(CO)_{12}Ru\{P(OMe)_3\}(\eta^6$-$C_6H_6$)] was also characterised spectroscopically, and it was suggested that in this compound the phosphine addition occurred at the Ru atom to generate an edge-bridged tetrahedral structure which subsequently underwent orthometallation to form the sterically-favoured thermodynamic product [13]. Conversely, in the reaction

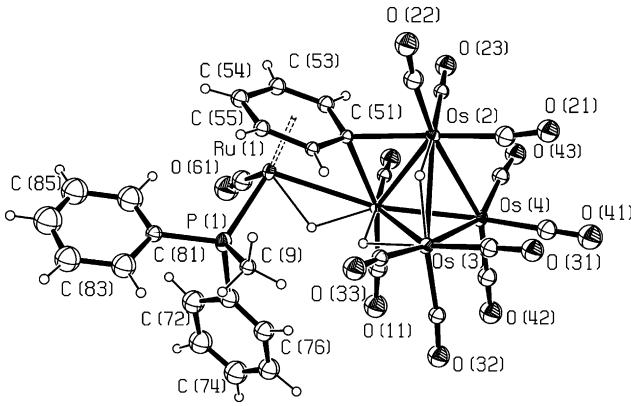

Fig. 4. Molecular structure of $[H_3Os_4Ru(CO)_{12}(\eta^6\text{-}C_6H_5)PPh_2Me]$ (**12**); the ellipsoids are shown at the 30% probability level.

with PPh_2Me, only the final product **6** could be identified.

To confirm the molecular structure of **12**, and compare the dimensions with $[H_3Os_4(CO)_{12}Ru\{P(OMe)_3\}(\mu_3\text{-}\sigma,\sigma,\eta^6\text{-}C_6H_5)]$, single crystals were grown by diffusion of hexane into a saturated solution in dichloromethane and a diffraction study undertaken. The molecular structure is shown in Fig. 4 and selected bond parameters are listed in Table 5. The hydride ligands were not located, but potential energy calculations [14] indicate that they bridge the same edges as in the $P(OMe)_3$ analogue, with one hydride spanning the 'spike' Os(1)–Ru(1) edge, and the other two bridging the Os(1)–Os(3) and Os(2)–Os(3) edges. The overall structure is very similar to the $P(OMe)_3$ compound, there being no significant differences in M–M distances in the 'spiked' tetrahedral metal core. The Os(1)–Ru(1)–P(1) angle is larger in the PPh_2Me [105.1(2)°] derivative than in the $P(OMe)_3$ [100.8(6)°] structure, although there are no significant differences in M–C distances involving the $\{\mu_3\text{-}\eta^6\text{-}C_6H_5\}$ ring.

2.5. Deprotonation of 1 and 2 and reaction with $[AuPPh_3]^+$

Clusters **1** and **2** may be deprotonated with NEt_3 in dichloromethane, at room temperature, to form the monoanion $[HOs_4M(CO)_{12}(\eta^6\text{-}C_6H_6)]^-$ and dianion $[Os_4M(CO)_{12}(\eta^6\text{-}C_6H_6)]^{2-}$ (M = Ru, Os). To isolate the monoanion, the solution was monitored by IR spectroscopy and the solvent was removed when the major absorptions had shifted halfway from the values in the starting material to those in the dianion $[Os_4M(CO)_{12}(\eta^6\text{-}C_6H_6)]^{2-}$ (M = Ru, Os). After washing the dry mixtures with hexane to remove the remaining base, excess $[AuPPh_3][NO_3]$, in CH_2Cl_2, was added and the mixture stirred for 1 h, yielding a monogold complexes $[HOs_4M(CO)_{12}(\eta^6\text{-}C_6H_6)AuPPh_3]$ (M = Os (**13**), Ru (**14**)) amongst other products (Scheme 1). In the case of **1**, small quantities of the known cluster

Table 5
Selected bond lengths (Å) and angles (°) for **12**

Os(1)–Os(2)	2.8111(15)	Os(1)–Os(3)	2.9600(18))
Os(1)–Os(4)	2.7693(16)	Os(1)–Ru(1)	3.006(2)
Os(2)–Os(3)	2.9704(15)	Os(2)–Os(4)	2.8330(16)
Os(3)–Os(4)	2.7893(16)	Ru(1)–P(1)	2.314(8)
Ru(1)–C(C_6H_5)	2.24(3)–2.38(2)	Os(3)–P(1)	2.394(9)
Os(1)–C(51)	2.31(2)	Os(2)–C(51)	2.56(4)
Os(1)–Ru(1)–P(1)	105.1(2)	P(1)–Ru(1)–C(51)	127.5(7)
Os(1)–Ru(1)–C(61)	106.4(11)	P(1)–Ru(1)–C(61)	89.4(11)
C(52)–C(51)–C(56)	115(2)	C(52)–C(51)–Os(1)	106.5(17)
C(56)–C(51)–Os(1)	113.2(16)	C(52)–C(51)–Os(2)	120.4(18)
C(56)–C(51)–Os(2)	117.3(19)		

$[H_4Os_5(CO)_{12}(\eta^6\text{-}C_6H_6)]$ [4] were also isolated. Clusters **13** and **14** have similar IR spectra and are structurally analogous. Both display singlets for the $\eta^6\text{-}C_6H_6$ protons and the hydride ligands in the ^1H NMR spectra; the chemical shifts of the latter are significantly downfield of those in the related compound $[HOs_5(CO)_{15}AuPPh_3]$ [18]. To confirm the structure of **13**, single crystals were grown by slow evaporation from dichloromethane–hexane solution and an X-ray analysis was undertaken. The molecular structure of **13** is shown in Fig. 5 and selected bond lengths and angles are given in Table 6. The cluster adopts a trigonal bipyramidal core with the $AuPPh_3$ moiety capping an Os_3 face, consistent with an electron count of 72 electrons, if the gold phosphine unit is considered as a one electron donor. Potential energy calculations indicate that the hydride ligand bridges an equatorial Os(1)–Os(3) edge and is coordinated to the metal that is also bonded to the C_6H_6 ligand. The arene ligand thus adopts the electronically favoured equatorial site, as in **4**, and a similar transformation must occur [13]. The structure is very similar to that of the parent

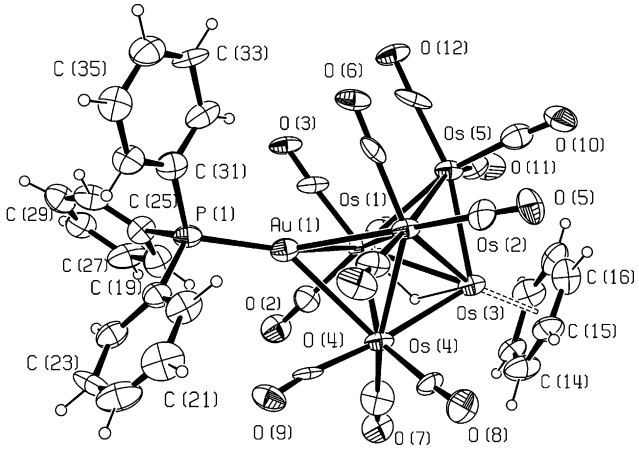

Fig. 5. Molecular structure of $[HOs_5(CO)_{12}(\eta^6\text{-}C_6H_6)AuPPh_3]$ (**13**); the ellipsoids are shown at the 30% probability level.

Table 6
Selected bond lengths (Å) and angles (°) for **13**

Os(1)–Os(2)	2.8915(15)	Os(1)–Os(3)	2.8535(19))
Os(1)–Os(4)	2.9043(16)	Os(1)–Os(5)	2.8071(19)
Os(1)–Au(1)	2.8420(19)	Os(2)–Os(3)	2.7903(19)
Os(2)–Os(4)	2.7414(18)	Os(2)–Os(5)	2.7785(18)
Os(2)–Au(1)	2.8188(19)	Os(3)–Os(4)	2.755(2)
Os(3)–Os(5)	2.7662(18)	Os(4)–Au(1)	3.020(2)
Os(3)–C(C_6H_6)	2.23(3)–2.26(4)	Au(1)–P(1)	2.285(7)
P(1)–Au(1)–Os(1)	144.92(17)	P(1)–Au(1)–Os(2)	147.86(19)
P(1)–Au(1)–Os(4)	143.0(2)		

cluster [$HOs_5(CO)_{15}AuPPh_3$] [18], although the bond lengths do differ in detail: those involving the Os bound to the arene ligand are significantly shorter (mean 2.792 Å) than those in the parent compound (mean 2.838 Å), and the edge lengthening effect of the bridging hydride ligand is less significant. The $AuPPh_3$ moiety bridges asymmetrically in each cluster, and the longest Au–Os bond in **13** is to the axial Os(4) atom, a trend that is also observed in the parent cluster.

2.6. Reactivity of *4* towards CO, H_2 and PPh_2Me

The equatorial isomer of [$H_2Os_5(CO)_{13}(\eta^6\text{-}C_6H_6)$] (**4**) is considerably less reactive towards electrophiles than the unstable axial isomer [$H_2Os_5(CO)_{13}(\eta^6\text{-}C_6H_6)$] (**1**). No reaction occurs when H_2 or CO gas is bubbled through solutions of **4** for 2 h at room temperature. Similarly, there is no reaction observed when PPh_2Me is stirred with a solution of **4** for 5 h at room temperature. However, after 5 days the addition product [$H_2Os_5(CO)_{13}(\eta^6\text{-}C_6H_6)PPh_2Me$] (**11**) was generated in approximately 30% yield alongside starting material and minor products in low yield. This suggests that **1** and **4** may be in equilibrium in solution, the small concentration of **4** present reacting with the phosphine.

2.7. Preparation of $[Os_4(CO)_{13}X]^-$ (X = Cl, Br, I)

The cluster anion $[Os_4(CO)_{13}X]^-$ (X = Cl (**15**), Br (**16**), I (**17**)) was obtained (as the $[(Ph_3P)_2N]^+$, $[Et_4N]^+$, or $[^tBuN]^+$ salt) by reaction of [$Os_3(CO)_{12}$] with the appropriate halide salt, in approximately 50% yield in each case. A single crystal of [$(Ph_3P)_2N$][$Os_4(CO)_{13}Cl$] (**15**) was grown by slow diffusion of methanol into a CH_2Cl_2 solution of the salt and the structure has been determined by single-crystal X-ray diffraction. The structure of the anion is shown in Fig. 6 while selected bond parameters are listed in Table 7. The cluster is isostructural with the Ru analogue [$(Ph_3P)_2N$][$Ru_4(CO)_{13}Cl$] [19]. The anion adopts a butterfly arrangement of the four Os atoms with the Cl ligand bridging the two wings of the butterfly, as the halide in $[Ru_4(CO)_{13}Cl]^-$ and the neutral butterfly

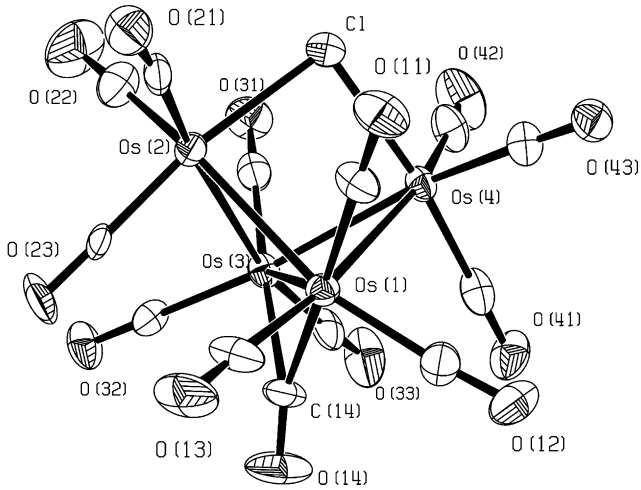

Fig. 6. The structure of the $[Os_4(CO)_{13}Cl]^-$ anion (**15**); the ellipsoids are shown at the 30% probability level.

Table 7
Selected bond lengths (Å) and angles (°) for **15**

Os(1)–Os(2)	2.823(1)	Os(1)–Os(3)	2.827(1)
Os(1)–Os(4)	2.823(1)	Os(2)–Os(3)	2.826(2)
Os(3)–Os(4)	2.811(2)	Os(2)–Cl	2.490(4)
Os(4)–Cl	2.481(6)	Os(1)–C(14)	2.12(2)
Os(3)–C(14)	2.24(2)		
Os(2)–Os(1)–Os(4)	78.7(1)	Os(2)–Os(3)–Os(4)	78.8(1)
Os(2)–Cl–Os(4)	92.1(2)	Os(1)–C(14)–O(14)	144.3(13)
Os(3)–C(14)–O(14)	134.9(14)		

clusters [$H_3Os_4(CO)_{12}Cl$] [20] and [$H_3Os_4(CO)_{12}I$] [21]. The Cl–Os distances are not significantly longer in **15** than those in [$H_3Os_4(CO)_{12}Cl$] although the Os–Cl–Os angle is greater in the latter [94.9 compared with 92.1(2)°] in **15**.

2.8. Reaction of $[Os_4(CO)_{13}X]^-$ (X = Cl, Br, I) with $[Ru(\eta^5\text{-}C_5H_5)(MeCN)_3]^+$ cation

The reaction of $[Os_4(CO)_{13}X]^-$ (X = Cl, Br, I) with 1 mol equiv. of [$Ru(\eta^5\text{-}C_5H_5)(MeCN)_3$][$PF_6$] in dichloromethane, at room temperature, yielded a single product [$HOs_4(CO)_{13}Ru(\eta^5\text{-}C_5H_5)$] (**18**) in each case (Scheme 2). The ^1H NMR spectrum indicated the presence of a bridging hydride ligand and one η^5-C_5H_5 ligand. The structure of **18** was determined by single-crystal X-ray diffraction and exhibits a trigonal bipyramidal cluster core with the 'RuCp' unit in one of the equatorial sites (Fig. 7); selected bond lengths and angles are given in Table 8 for the two similar but independent molecules in the asymmetric unit. The metal–metal distances range from 2.727(2) to 2.987(2) Å, which is comparable to the ranges in related arene complexes [$H_4Os_4(CO)_{11}Ru(\eta^5\text{-}C_6H_6)$] [4] and

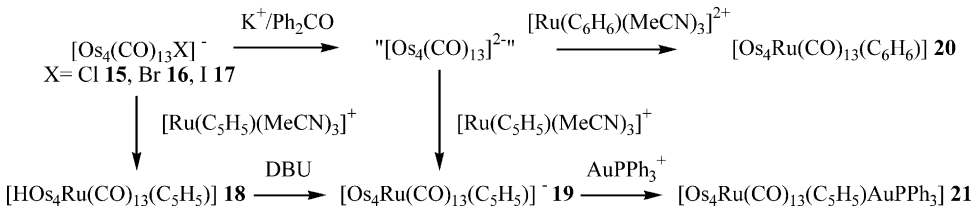

Scheme 2.

$[H_2Os_5(CO)_{12}(\eta^5\text{-}C_6H_5Me)]$ (**5**) in which the arene ligands are also coordinated in the electronically-favoured equatorial site [12,13]. However, in this case the equatorial isomer is probably the kinetic as well as the thermodynamic product, as the butterfly anion is 'capped' without any cluster rearrangement occurring. The longest distances involve the Ru atom, which has the highest connectivity and formal electron count. Potential energy calculations [14] indicate that the hydride ligand bridges the longest Os(1a)–Ru(1a) edge. One CO ligand is semi-bridging from Ru(1a) to Os(3a) [Ru(1a)–C(13a)–O(13a) 164.2(16)°, Os(3a)–C(13a)–O(13a) 117.8(15)°] whilst the others are *pseudo*-linearly coordinated.

2.9. Reactivity of $[HOs_4(CO)_{13}Ru(\eta^5\text{-}C_5H_5)]$ (18) towards phosphines

Unlike $[H_2Os_5(CO)_{12}(\eta^6\text{-}C_6H_6)]$ (**4**), which undergoes a nucleophilic addition reaction with phosphines to form the edge-bridged tetrahedral cluster $[H_2Os_5(CO)_{12}(\eta^5\text{-}C_6H_5Me)L]$ (L = PPh_2Me) (**11**) after 5 days, reaction of **18** with L = PPh_3, $P(OMe)_3$, PPh_2Me, in CH_2Cl_2, at room temperature, for 5 days led to the recovery of the starting material. When the reaction was carried out in dichloromethane, under reflux, cluster degradation occurred and the only products were obtained in very low yield.

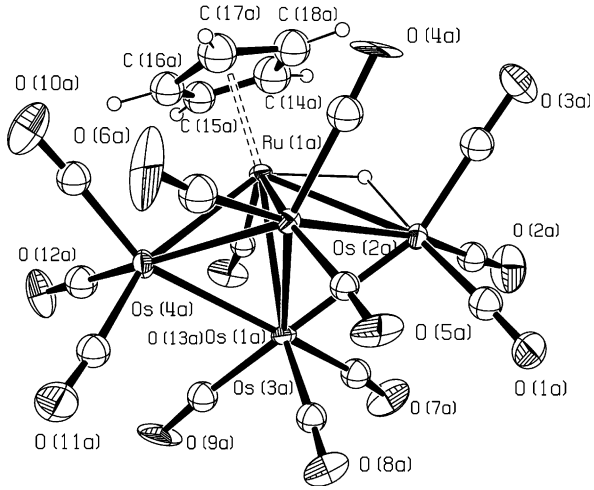

Fig. 7. The structure of one of the two independent but structurally similar molecules of $[HOs_4(CO)_{13}Ru(\eta^5\text{-}C_5H_5)]$ (**18**); the ellipsoids are shown at the 30% probability level.

Table 8
Selected bond lengths (Å) and angles (°) for **18**

Os(1a)–Os(2a)	2.7697(14)	Os(1b)–Os(2b)	2.7759(14)
Os(1a)–Os(3a)	2.7918(13)	Os(1b)–Os(3b)	2.7894(12)
Os(1a)–Ru(1a)	2.986(2)	Os(1b)–Ru(1b)	2.982(2)
Os(2a)–Os(3a)	2.7541(12)	Os(2b)–Os(3b)	2.7556(12)
Os(2a)–Os(4a)	2.7266(12)	Os(2b)–Os(4b)	2.7413(12)
Os(2a)–Ru(1a)	2.824(2)	Os(2b)–Ru(1b)	2.810(2)
Os(3a)–Os(4a)	2.737(2)	Os(3b)–Os(4b)	2.7353(15)
Os(4a)–Ru(1a)	2.876(2)	Os(4b)–Ru(1b)	2.880(2)
Ru(1a)–C(C_5H_5)	2.21(3)–2.27(3)	Ru(1b)–C(C_5H_5)	2.19(3)–2.28(3)
Os(3a)–C(13a)	2.60(2)	Os(3b)–C(13b)	2.66(2)
Ru(1a)–C(13a)	1.85(3)	Ru(1b)–C(13b)	1.90(2)
Os(3a)–C(13a)–O(13a)	119(2)	Os(3b)–C(13b)–O(13b)	119(2)
Ru(1a)–C(13a)–O(13a)	163(2)	Ru(1b)–C(13b)–O(13b)	164(2)

2.10. Deprotonation of $[HOs_4(CO)_{13}Ru(\eta^5\text{-}C_5H_5)]$ (18) and reaction with $[AuPPh_3]^+$

Cluster **18** may be deprotonated with DBU, in dichloromethane, to generate the monoanionic cluster $[Os_4(CO)_{13}Ru(\eta^5\text{-}C_5H_5)]^-$ (**19**), that has been characterised by IR, ^1H NMR spectroscopy and (−) FAB mass spectrometry (Table 1). The weak absorption at 1722 cm^{-1} indicates that a (semi)-bridging carbonyl is present as in **18**. When treated with 1.5 mol equiv. of $[AuPPh_3][NO_3]$, the neutral cluster $[Os_4(CO)_{13}Ru(\eta^5\text{-}C_5H_5)AuPPh_3]$ (**20**) is produced in good yield, as characterised by ^1H NMR and IR spectroscopy (Table 1). The structure was determined by X-ray crystallography and showed a trigonal bipyramidal metal core similar to that in **18**, with the '$AuPPh_3$' unit capping one of the Os_3 triangular faces (Fig. 8). Selected bond parameters are listed in Table 9. No rearrangement of the Os_4Ru core occurs and the $Ru(\eta^5\text{-}C_5H_5)$ group remains at the equatorial site. The metal core geometry is thus similar to that observed in the related face-capped trigonal bipyramidal clusters $[HOs_5(CO)_{15}AuPPh_3]$ [18] and $[HOs_5(CO)_{12}(\eta^6\text{-}C_6H_6)AuPPh_3]$ (**13**), except that a semi-bridging CO ligand (Os(2)–C(23) 2.56(2) Å, Ru(1)–C(23) 1.81(2) Å) replaces the μ_2-H ligand in **20**. The $AuPPh_3$ group in **20** [Os–Au 2.788(3)–2.936(2) Å] also bridges asymmetri-

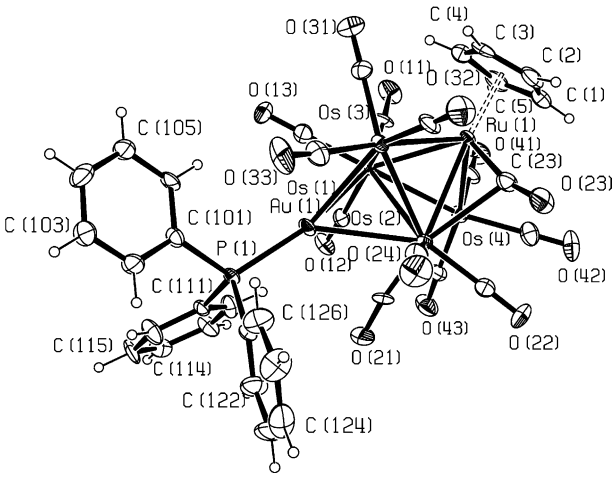

Fig. 8. Molecular structure of $[Os_4(CO)_{13}Ru(\eta^5\text{-}C_5H_5)AuPPh_3]$ (**20**); the ellipsoids are shown at the 30% probability level.

Table 9
Selected bond lengths (Å) and angles (°) for **20**

Os(1)–Os(2)	2.827(3)	Os(1)–Os(3)	2.799(2)
Os(1)–Os(4)	2.797(2)	Os(1)–Ru(1)	2.814(4)
Os(2)–Os(3)	2.872(3)	Os(2)–Os(4)	2.764(3)
Os(2)–Ru(1)	2.850(3)	Os(3)–Ru(1)	2.746(2)
Os(4)–Ru(1)	2.764(2)	Os(1)–Au(1)	2.788(3)
Os(2)–Au(1)	2.936(2)	Os(3)–Au(1)	2.799(2)
Ru(1)–C(C_5H_5)	2.250(13)–2.294(12)	Au(1)–P(1)	2.282(3)
Os(2)–C(23)	2.562(13)	Ru(1)–C(23)	1.814(12)
Os(2)–C(23)–O(23)	116.6(10)	Ru(1)–C(23)–O(23)	164.1(12)

cally, suggesting that the Au–Os bonding is relatively 'soft'. The capping Au atom has the effect of increasing axial–equatorial distances relative to those in **18**, whereas the absence of the bridging hydride decreases the coordination number and formal electron count of the equatorial Ru atom such that it forms much shorter bonds than those in **18** that are comparable in length to the unbridged Os–Os axial–equatorial distances.

2.11. Reduction of $[Os_4(CO)_{13}X]^-$ (X = Cl (**15**), Br (**16**), I (**17**))

Reduction of the butterfly clusters $[Os_4(CO)_{13}X]^-$ (X = Cl, Br, I) with potassium diphenylketyl in THF, at room temperature, generates the same reduced species with IR absorptions at 1987(s), 1964(m) and 1924(w) cm^{-1}, indicating that there is a higher anionic charge on the common reduced cluster [22]. A tentative formulation is $[Os_4(CO)_{13}]^{2-}$, i.e., loss of halide and a two-electron reduction has occurred. The dianion $[Os_4(CO)_{13}]^{2-}$ has not been structurally characterised, but on the basis of electron-counting rules would be expected to have a tetrahedral core as in the related $60e^-$ monoanion $[HOs_4(CO)_{13}]^-$ (structurally characterised as its $[(Ph_3P)_2N]^+$ salt) [23].

2.12. Reaction of $[Os_4(CO)_{13}]^{2-}$ with $[Ru(C_5H_5)(MeCN)_3]^+$ and $[Ru(\eta^6\text{-}C_6H_6)(MeCN)_3]^{2+}$

The reaction of $[Ru(\eta^5\text{-}C_5H_5)(MeCN)_3][PF_6]$ with $[Os_4(CO)_{13}]^{2-}$ yields the monoanion $[Os_4(CO)_{13}Ru(\eta^5\text{-}C_5H_5)]^-$ (**19**), described above, directly, as identified by its IR and ^1H NMR spectra (Scheme 2). Similarly, ionic coupling with the dicationic species $[Ru(\eta^6\text{-}C_6H_6)(MeCN)_3][BF_4]_2$ with $[Os_4(CO)_{13}]^{2-}$ yields the neutral cluster $[Os_4(CO)_{13}Ru(\eta^6\text{-}C_6H_6)]$ (**21**). The structure of **21** has been determined by single crystal X-ray diffraction showing the trigonal pyramidal Os_4Ru metal core with the $Ru(\eta^6\text{-}C_6H_6)$ unit (mean Ru–C distance 2.29 Å) in the electronically-favoured equatorial site as in **18** and **20**. The ligand polyhedron is also very similar, although the semi-bridging CO ligand is more symmetric [Ru–C(22)–O(22) 143(2)°, Os(2)–C(22)–O(22) 132(2)°]; this semi-bridging ligand allows the redistribution of the electron density arising from the arene fragment. As in **18**, the Ru–Os bonds are longer than the Os–Os bonds, and the shortest bonds are between the formally $17e^-$ Os(3), Os(4) and 'electron precise' equatorial Os(1), Os(2) vertices. A point of interest is that only the thermodynamically favoured product with the arene in the equatorial position is observed. The axial isomer which might be expected to result from the initial 'capping' of an Os_3 face of $[Os_4(CO)_{13}]^{2-}$ is not observed, unlike the reaction of '$Os(C_6H_6)^{2+}$' with $[H_2Os_4(CO)_{12}]^{2-}$ where the axial product **1** is observed initially but transforms to the more stable equatorial isomer **4**, possibly via a Berry pseudo-rotation mechanism [12,13].

2.13. Reactivity of $[Os_4(CO)_{13}Ru(\eta^6\text{-}C_6H_6)]$ (**21**) with phosphines

The cluster $[Os_4(CO)_{13}Ru(\eta^6\text{-}C_6H_6)]$ (**21**), as **18**, is not susceptible to nucleophilic substitution and no reaction was observed with the phosphines PPh_3, $P(OMe)_3$, PPh_2Me at room temperature, and only trace products in very low yield were observed after heating a CH_2Cl_2 solution under reflux for 12 h (Table 10, Fig. 9).

Table 10
Selected bond lengths (Å) and angles (°) for **21**

Os(1)–Os(2)	2.775(2)	Os(1)–Os(3)	2.704(2)
Os(1)–Os(4)	2.727(2)	Os(1)–Ru(1)	2.787(2)
Os(2)–Os(3)	2.822(2)	Os(2)–Os(4)	2.782(2)
Os(2)–Ru(1)	2.799(2)	Os(3)–Ru(1)	2.792(2)
Os(4)–Ru(1)	2.780(2)	Ru(1)–C(C_6H_6)	2.25(3)–2.32(2)
Os(2)–C(22)	2.19(2)	Ru(1)–C(22)	1.92(2)
Os(2)–C(22)–O(22)	131(2)	Ru(1)–C(22)–O(22)	143(2)

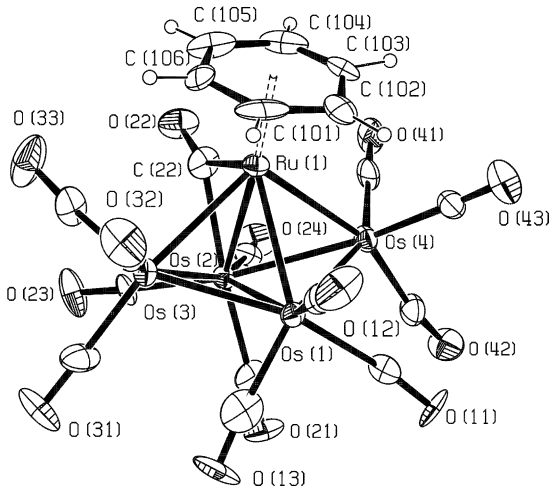

Fig. 9. Molecular structure of $[Os_4(CO)_{13}Ru(\eta^6\text{-}C_6H_6)]$ (**21**); the ellipsoids are shown at the 30% probability level.

3. Experimental

All the reactions were performed under an atmosphere of dry, oxygen-free nitrogen using standard Schlenk techniques. Technical grade solvents were purified by distillation over the appropriate drying agents and under an inert nitrogen atmosphere prior to use. Routine separation of products was performed by thin-layer chromatography (TLC) using commercially-prepared glass plates, pre-coated to 0.25 mm thickness with Merck Kieselgel 60 F_{254}, as supplied by Merck, or using laboratory-prepared glass plates coated to 1 mm thickness with Merck Kieselgel 60 F_{254}. The complexes $[H_2Os_4(CO)_{13}]$ [24], $[M(\eta^6\text{-}C_6H_6)(MeCN)_3]$ (M = Os [25], Ru [26]) $[Os(\eta^6\text{-}C_6H_5Me)Cl_2]$ [27] $[AuPPh_3][NO_3]$ [28], $[(Ph_3P)_2N][Os_4(CO)_{13}Cl]$ [29], $[Os_3(CO)_{12}]$ [30] and $[Ru(\eta^5\text{-}C_5H_5)(CH_3CN)_3]$ [31] were prepared by literature procedures. Other chemicals were used as purchased without further purification.

The FAB MS were recorded using a Kratos model 902 spectrometer, IR spectra on a Perkin–Elmer 1710 FT IR spectrometer, using 0.5 mm NaCl or CaF_2 cells, and ^1H, ^{31}P and ^{13}C NMR spectra on a Bruker WH 250 MHz or WH 400 MHz spectrometer. The internal reference used for the ^{31}P NMR spectra is H_3PO_4.

3.1. Preparations

3.1.1. $K_2[H_2Os_4(CO)_{12}]$

To a solution of $[H_2Os_4(CO)_{13}]$ (50 mg, 0.044 mmol) in THF (20 ml), cooled to −60 °C using a dry ice–acetone bath, was added a solution of K/Ph_2CO dropwise whilst stirring. When the blue colour of K/Ph_2CO persisted the cooling bath was removed and the solution stirred until it turned a yellow colour. The solvent was removed under vacuo to leave $K_2[H_2Os_4(CO)_{12}]$ as an orange oil which was used without further purification.

3.1.2. $[H_2Os_5(CO)_{12}(\eta^6\text{-}C_6H_6)]$ (**1**)

CH_2Cl_2 (20 ml) was added to a sealed flask containing freshly prepared $K_2[H_2Os_4(CO)_{12}]$ (50 mg, 0.042 mmol) and an excess of $[Os(\eta^6\text{-}C_6H_6)(MeCN)_3][BF_4]_2$ (33 mg, 0.068 mmol). The mixture was stirred for 20 min to give a dark red solution which was concentrated and then chromatographed by TLC using CH_2Cl_2:hexane (3:2) as eluent to give a maroon compound $[H_2Os_5(CO)_{12}(\eta^6\text{-}C_6H_6)]$ (**1**) as the major product. In this preparation, care was taken not to leave the compound long on the TLC plate as it tended to convert to isomer **4**.

3.1.3. $[H_2Os_4Ru(CO)_{12}(\eta^6\text{-}C_6H_6)]$ (**2**)

CH_2Cl_2 (20 ml) was added to a sealed flask containing freshly prepared $K_2[H_2Os_4(CO)_{12}]$ (50 mg, 0.042 mmol) and an excess of $[Ru(\eta^6\text{-}C_6H_6)(MeCN)_3][BF_4]_2$ (27 mg, 0.068 mmol). The mixture was warmed slightly using a water bath and stirred for 20 min to give a brown solution which was concentrated and then chromatographed by TLC using CH_2Cl_2:hexane (3:2) as eluent to give a purple compound $[H_2Os_4Ru(CO)_{12}(\eta^6\text{-}C_6H_6)]$ (**2**) as the major product.

3.1.4. $[H_2Os_5(CO)_{12}(\eta^6\text{-}C_6H_5Me)]$ (**3**)

$[Os(C_6H_5Me)Cl_2]_2$ (20 mg, 0.028 mmol) was suspended in CH_2Cl_2 and $Ag(CF_3SO_3)$ (40 mg, 0.183 mmol) was added to it and the mixture stirred for 30 min. The solution was filtered through celite to remove the AgCl precipitate and the colourless filtrate was collected into a flask containing freshly prepared $K_2[H_2Os_4(CO)_{12}]$ (50 mg, 0.042 mmol). The mixture was stirred for 15 min to give a brown solution which was concentrated and immediately chromatographed by TLC using CH_2Cl_2:hexane (3:2) as eluent to give a purple compound $[H_2Os_5(CO)_{12}(\eta^6\text{-}C_6H_5Me)]$ (**3**) as the major product.

3.1.5. $[H_2Os_5(CO)_{12}(\eta^6\text{-}C_6H_6)]$ (**4**)

The maroon isomer $[H_2Os_5(CO)_{12}(\eta^6\text{-}C_6H_6)]$ (**1**) (30 mg, 0.022 mmol) was left for 24 h in CH_2Cl_2 (3 ml) and the resultant brown solution was chromatographed on thin TLC plates using CH_2Cl_2:hexane as eluent to give three bands. The top green–brown band was identified as $[H_2Os_5(CO)_{13}(\eta^6\text{-}C_6H_6)]$ (**6**) in 40% yield (12.5 mg, 0.0088 mmol), the middle band (10%, 3 mg, 0.0022 mmol) was found to be the starting material **1**, and the lower band in 40% yield (12.0 mg, 0.0088 mmol) was identified as $[H_2Os_5(CO)_{12}(\eta^6\text{-}C_6H_6)]$ (**4**).

3.1.6. $[H_2Os_5(CO)_{12}(\eta^6\text{-}C_6H_5Me)]$ (**5**)

The purple isomer $[H_2Os_5(CO)_{12}(\eta^6\text{-}C_6H_5Me)]$ (**3**) (30 mg, 0.022 mmol) was left for 24 h in CH_2Cl_2 (3 ml) and the resultant brown solution was chromatographed on

thin TLC plates using CH_2Cl_2:hexane as eluent to give three bands. The top green–brown band was identified as $[H_2Os_5(CO)_{13}(\eta^6\text{-}C_6H_5Me)]$ (**8**) in 40% yield (12.4 mg, 0.0088 mmol), the middle band (10%, 3 mg, 0.0022 mmol) was found to be the starting material **3**, and the lower band in 40% yield (12 mg, 0.0088 mmol) was identified as $[H_2Os_5(CO)_{12}(\eta^6\text{-}C_6H_5Me)]$ (**5**).

3.1.7. $[H_2Os_5(CO)_{13}(\eta^6\text{-}C_6H_6)]$ (6)

Carbon monoxide was bubbled through a CH_2Cl_2 (20 ml) solution of freshly prepared $[H_2Os_5(CO)_{12}(\eta^6\text{-}C_6H_6)]$ (**1**) (20 mg, 0.015 mmol) at room temperature (r.t.) for 30 min and the solution changed from maroon to green–brown. The solution was concentrated and chromatographed using CH_2Cl_2:hexane (1:1) as eluent to give a quantitative yield (20.4 mg, 0.015 mmol) of $[H_2Os_5(CO)_{13}(\eta^6\text{-}C_6H_6)]$ (**6**).

3.1.8. $[H_2Os_4Ru(CO)_{13}(\eta^6\text{-}C_6H_6)]$ (7)

Carbon monoxide was bubbled through a CH_2Cl_2 (20 ml) solution of freshly prepared $[H_2Os_4Ru(CO)_{12}(\eta^6\text{-}C_6H_6)]$ (**2**) (25 mg, 0.020 mmol) at r.t. for 30 min and the solution changed from purple to red. The solution was concentrated and chromatographed using CH_2Cl_2:hexane (1:1) as eluent to give a quantitative yield (26 g, 0.020 mmol) of $[H_2Os_4Ru(CO)_{13}(\eta^6\text{-}C_6H_6)]$ (**7**). {*Anal*. Found: C, 17.44; H, 0.58. Calc. for $[H_2Os_4Ru(CO)_{13}(\eta^6\text{-}C_6H_6)]$: C, 17.47, H 0.62%}.

3.1.9. $[H_2Os_5(CO)_{13}(\eta^6\text{-}C_6H_5Me)]$ (8)

Carbon monoxide was bubbled through a CH_2Cl_2 (20 ml) solution of freshly prepared $[H_2Os_5(CO)_{12}(\eta^6\text{-}C_6H_5Me)]$ (**3**) (20 mg, 0.014 mmol) at r.t. for 30 min and the solution changed from purple to green–brown. The solution was concentrated and chromatographed on thin plates using CH_2Cl_2:hexane (1:1) as eluent to give a top green–brown band of $[H_2Os_5(CO)_{13}(\eta^6\text{-}C_6H_5Me)]$ (**8**) in 70% yield (14 mg, 0.010 mmol) and a bottom brown band of $[H_2Os_5(CO)_{12}(\eta^6\text{-}C_6H_5Me)]$ (**5**) in 30% yield (6 mg, 0.004 mmol).

3.1.10. $[H_4Os_5(CO)_{12}(\eta^6\text{-}C_6H_6)]$ (9)

H_2 was bubbled through a CH_2Cl_2 (20 ml) solution of freshly prepared $[H_2Os_5(CO)_{12}(\eta^6\text{-}C_6H_6)]$ (**1**) (20 mg, 0.015 mmol) at r.t. for 2 h and the solution changed colour from maroon to green. The solution was chromatographed on thin plates using CH_2Cl_2:hexane (1:1) as eluent to give one major band $[H_4Os_5(CO)_{12}(\eta^6\text{-}C_6H_6)]$ (**9**) in 80% yield (16.0 mg, 0.012 mmol). {*Anal*. Found: C, 25.7; H, 0.7. Calc. for $[H_2Os_5(CO)_{12}(\eta^6\text{-}C_6H_6)]$: C, 15.8; H, 0.7%}.

3.1.11. $[H_4Os_4Ru(CO)_{12}(\eta^6\text{-}C_6H_6)]$ (10)

H_2 was bubbled through a CH_2Cl_2 (20 ml) solution of freshly prepared $[H_2Os_4Ru(CO)_{12}(\eta^6\text{-}C_6H_6)]$ (**2**) (25 mg, 0.020 mmol) at r.t. for 2 h and the solution changed colour from purple to green. The solution was chromatographed on thin plates using CH_2Cl_2:hexane (1:1) as eluent to give one major green band $[H_4Os_4Ru(CO)_{12}(\eta^6\text{-}C_6H_6)]$ (**10**) in 80% yield (20 mg, 0.016 mmol).

3.1.12. $[H_2Os_5(CO)_{12}(\eta^6\text{-}C_6H_6)PPh_2Me]$ (11)

A drop of PPh_2Me was added to a CH_2Cl_2 (20 ml) solution of freshly prepared $[H_2Os_5(CO)_{12}(\eta^6\text{-}C_6H_6)]$ (**1**) (20 mg, 0.015 mmol) at r.t. The solution rapidly turned brown and after 15 min the solution was concentrated and chromatographed on TLC using CH_2Cl_2:hexane (3:7) as eluent to give one major green–brown band of $[H_2Os_5(CO)_{12}(\eta^6\text{-}C_6H_6)PPh_2Me]$ (**11**) in 85% yield (19.8 mg, 0.013 mmol). {*Anal*. Found: C, 24.00; H, 1.39. Calc. for $[H_2Os_5(CO)_{12}(\eta^6\text{-}C_6H_6)PPh_2Me]$: C, 23.75; H 1.35%}.

3.1.13. $[H_3Os_4Ru(CO)_{12}(\eta^6\text{-}C_6H_5)PPh_2Me]$ (12)

A drop of PPh_2Me was added to a CH_2Cl_2 (20 ml) solution of freshly prepared $[H_2Os_4Ru(CO)_{12}(\eta^6\text{-}C_6H_6)]$ (**2**) (25 mg, 0.020 mmol) at r.t. The solution rapidly turned orange and after 15 min the solution was concentrated and chromatographed on TLC using CH_2Cl_2:hexane (3:7) as eluent to give one major orange band of $[H_3Os_4Ru(CO)_{12}(\eta^6\text{-}C_6H_5)PPh_2Me]$ (**12**) in 85% yield (23.6 mg, 0.016 mmol). {*Anal*. Found: C, 25.29; H, 1.42. Calc. for $[H_3Os_4Ru(CO)_{12}(\eta^6\text{-}C_6H_5)PPh_2Me]$: C, 25.19; H 1.43%}.

3.1.14. $[HOs_5(CO)_{12}(\eta^6\text{-}C_6H_6)AuPPh_3]$ (13)

A drop of NEt_3 was added to a stirred CH_2Cl_2 (20 ml) solution of freshly prepared $[H_2Os_5(CO)_{12}(\eta^6\text{-}C_6H_6)]$ (**1**) (20 mg, 0.015 mmol) at r.t. and the solution monitored by IR until the major peaks had shifted to values intermediate between the starting material and the dianion. The solvent was removed under vacuum to leave a brown oil which was washed several times with hexane to remove excess NEt_3. Excess of $AuPPh_3NO_3$ (10 mg, 0.020 mmol) and CH_2Cl_2 (20 ml) was added to the brown oil and the mixture stirred for 1 h after which the solution was concentrated and chromatographed by TLC using CH_2Cl_2:hexane (3:2) as eluent to give a top orange band $[HOs_5(CO)_{12}(\eta^6\text{-}C_6H_6)AuPPh_3]$ (**13**) in 40% yield (11.0 mg, 0.006 mmol), a second dark brown band in 20% yield (tentatively formulated as $[Os_5(CO)_{12}(\eta^6\text{-}C_6H_6)(AuPPh_3)_2]$, 6.8 mg, 0.003 mmol), a third green band in 15% yield $[H_4Os_5(CO)_{12}(\eta^6\text{-}C_6H_6)]$ (**9**) (3 mg, 0.002 mmol) and an unidentified polar band.

3.1.15. $[HOs_4Ru(CO)_{12}(\eta^6\text{-}C_6H_6)AuPPh_3]$ (14)

A drop of NEt_3 was added to a stirred CH_2Cl_2 (20 ml) solution of freshly prepared $[H_2Os_4Ru(CO)_{12}(\eta^6\text{-}C_6H_6)]$ (**2**) (25 mg, 0.020 mmol) at r.t. and the solution monitored by IR until the major peaks had shifted to values intermediate between the starting material and

the dianion. The solvent was removed under vacuum to leave a brown oil which was washed several times with hexane to remove excess NEt_3. Excess of $AuPPh_3NO_3$ (15 mg, 0.029 mmol) and CH_2Cl_2 (20 ml) was added to the brown oil and the mixture stirred for 1 h after which the solution was concentrated and chromatographed by TLC using CH_2Cl_2:hexane (3:2) as eluent to give a top orange–brown band $[HOs_4Ru(CO)_{12}(\eta^6\text{-}C_6H_6)AuPPh_3]$ (**14**) in 70% yield (24.3 mg, 0.014 mmol) and an unidentified polar band.

3.1.16. Reaction of $[H_2Os_5(CO)_{12}(\eta^6\text{-}C_6H_6)]$ (4) with PPh_2Me

To a solution of $[H_2Os_5(CO)_{12}(\eta^6\text{-}C_6H_6)]$ (**4**) (20 mg, 0.015 mmol) in CH_2Cl_2 (30 ml) was added PPh_2Me (10 mg, 0.050 mmol) and the solution stirred for 5 h at r.t., after which no change in the IR absorptions were observed. Subsequently, the solution was stirred for a further 5 days, after which time the solution was concentrated and chromatographed on TLC using CH_2Cl_2:hexane (3:7) as eluent to give one major green–brown band of $[H_2Os_5(CO)_{12}(\eta^6\text{-}C_6H_6)PPh_2Me]$ (**11**) in 30% yield (7.0 mg, 0.004 mmol) beside the starting material and decomposition products.

3.1.17. $[HOs_4(CO)_{13}Ru(\eta^5\text{-}C_5H_5)]$ (18)

To a solution of $[(Ph_3P)_2N][Os_4(CO)_{13}Cl]$ (50 mg, 0.029 mmol), $[(Ph_3P)_2N][Os_4(CO)_{13}Br]$ (50 mg, 0.029 mmol), or $[(Ph_3P)_2N][Os_4(CO)_{13}I]$ (50 mg, 0.028 mmol), in 30 ml CH_2Cl_2 was added 1 mol equiv. of $[Ru(\eta^5\text{-}C_5H_5)(MeCN)_3][PF_6]$ (8.8 mg, 0.030 mmol). The solution was stirred for 30 min and the solvent removed under vacuo prior to TLC using CH_2Cl_2:hexane (1:1) as eluent to give a dark green major product $[HOs_4(CO)_{13}Ru(\eta^5\text{-}C_5H_5)]$ (**18**) ($R_f = 0.75$) in 40% yield (15.2 mg, 0.012 mmol). {*Anal*. Found: C, 16.71; H, 0.44. Calc. for $[HOs_4(CO)_{13}Ru(\eta^5\text{-}C_5H_5)]$: C, 16.7; H 0.5%}.

3.1.18. Reaction of $[HOs_4(CO)_{13}Ru(\eta^5\text{-}C_5H_5)]$ (18) with phosphines

To a solution of $[HOs_4(CO)_{13}Ru(\eta^5\text{-}C_5H_5)]$ (**15**) (20 mg, 0.016 mmol) in CH_2Cl_2 (30 ml) was added PPh_3 (10 mg, 0.038 mmol) and the solution stirred for 5 days, after which no change in the IR absorptions were observed. Subsequently, the solution was heated under reflux for 30 min, the solvent evaporated and the residue chromatographed using CH_2Cl_2:hexane as eluent, but no products could be isolated. The same method was applied to $P(OMe)_3$ (5 mg, 0.054 mmol) and PPh_2Me (10 mg, 0.050 mmol) with the same result.

3.1.19. $[Os_4(CO)_{13}Ru(\eta^5\text{-}C_5H_5)AuPPh_3]$ (20)

To a solution of $[HOs_4(CO)_{13}Ru(\eta^5\text{-}C_5H_5)]$ (**15**) (25 mg, 0.019 mmol) in THF was added two drops of 1,8-diazabicyclo[5.4.0]undec-7-ene (DBU). Change in IR absorption bands indicated the presence of the deprotonated species $[Os_4(CO)_{13}Ru(\eta^5\text{-}C_5H_5)]^-$ (**19**). Subsequent addition of 1.5 mol equiv. of $[AuPPh_3][NO_3]$ (15.7 mg, 0.028 mmol) was followed by stirring for a further 20 min. After removal of solvent, the solid residue was chromatographed using CH_2Cl_2–hexane (1:1) as eluent. The red–brown band 20 ($R_f = 0.6$) was obtained in 60% yield (20.3 mg, 0.012 mmol). {*Anal*. Found: C, 24.86; H, 1.28. Calc. for $[Os_4(CO)_{13}Ru(\eta^5\text{-}C_5H_5)AuPPh_3]$: C, 24.71; H, 1.14%}.

3.1.20. Reduction of $[Os_4(CO)_{13}X]^-$ ($X = Cl, Br, I$)

$[(Ph_3P)_2N][Os_4(CO)_{13}Cl]$ (50 mg, 0.029 mmol) $[(Ph_3P)_2N][Os_4(CO)_{13}Br]$ (50 mg, 0.029 mmol) or $[(Ph_3P)_2N][Os_4(CO)_{13}I]$ (50 mg, 0.028 mmol), respectively, were dissolved in THF. Freshly prepared potassium diphenylketyl was added to the solution until the blue colour persisted. The solution was stirred until it turned orange, and the solvent removed under vacuo to obtain a dark orange residue that was used without further purification.

3.1.21. $[Os_4(CO)_{13}Ru(\eta^5\text{-}C_5H_5)]^-$ (19)

Deoxygenated freshly distilled dichloromethane (30 ml) was added to the sealed Schlenk flask containing residue from the reduction of $[Os_4(CO)_{13}X]^-$ (X = Cl, Br, I; 0.029 mmol) and 2.5 mol equiv. of $[Ru(\eta^5\text{-}C_5H_5)(MeCN)_3][PF_6]$ (25 mg, 0.072 mmol) was added. The solution was stirred for 30 min, the solvent evaporated and the residue chromatographed using CH_2Cl_2 as eluent. The green–brown band ($R_f = 0.7$) was obtained as a major product (30% yield) and the anion characterised spectroscopically as $[Os_4(CO)_{13}Ru(\eta^5\text{-}C_5H_5)]^-$ (**19**).

3.1.22. $[Os_4(CO)_{13}Ru(\eta^6\text{-}C_6H_6)]$ (21)

Deoxygenated freshly distilled dichloromethane (30 ml) was added to the sealed Schlenk flask containing residue from the reduction of $[Os_4(CO)_{13}X]^-$ (X = Cl, Br, I; 0.029 mmol) and 1.5 mol equiv. of $[Ru(\eta^6\text{-}C_6H_6)(MeCN)_3][BF_4]_2$ (17 mg, 0.044 mmol) was added. The solution was stirred for 30 min, the solvent removed under vacuo and the residue chromatographed using CH_2Cl_2:hexane as eluent. The dark green band ($R_f = 0.7$) was obtained as the major product in 30% yield (11.5 mg, 0.009 mmol) and characterised spectroscopically as $[Os_4(CO)_{13}Ru(\eta^6\text{-}C_6H_6)]$ (**21**). {*Anal*. Found: C, 17.31; H, 0.40. Calc. for $[Os_4(CO)_{13}Ru(\eta^6\text{-}C_6H_6)]$: C, 17.50; H 0.46%}.

3.1.23. Reaction of $[Os_4(CO)_{13}Ru(\eta^6\text{-}C_6H_6)]$ (21) with phosphines

To a solution of $[Os_4(CO)_{13}Ru(\eta^6\text{-}C_6H_6)]$ (**21**) (20 mg, 0.015 mmol) in CH_2Cl_2 (30 ml), PPh_3 (10 mg, 0.038 mmol) was added and the solution stirred for 5 days, after which no change in the IR absorptions were observed. Subsequently, the solution was heated under

Table 11
Crystal data, data collection, structure and refinement parameters for **5**, **7**, **11**, **12**, **13**, **15**, **18**, **20**, **21**

Complex	**5**	**7**	**11**	**12**	**13**	**15**	**18**	**20**	**21**
Molecular formula	$C_{19}H_{10}O_{12}Os_5$	$C_{19}H_8O_{13}OsRu$	$C_{31}H_{21}O_{12}Os_5P\cdot 0.25\ CH_2Cl_2$	$C_{31}H_{21}O_{12}Os_4Pru$	$C_{36}H_{22}AuO_{12}Os_5P$	$C_{49}H_{30}ClNO_{13}Os_4P$	$C_{18}H_6O_{13}Os_4Ru$	$C_{36}H_{20}AuO_{13}Os_4PRu\cdot 0.5(CH_2Cl_2)$	$C_{19}H_6O_{13}Os_4Ru$
M	1381.27	1306.12	1588.68	1478.32	1825.47	1698.9	1292.10	1792.79	1304.11
Crystal system	orthorhombic	monoclinic	orthorhombic	orthorhombic	triclinic	triclinic	triclinic	triclinic	Monoclinic
a (Å)	11.738(6)	11.246(4)	12.811(3)	22.337(7)	12.254(5)	11.456(4)	8.918(2)	10.099(9)	9.719(4)
b (Å)	11.860(4)	15.228(5)	20.892(4)	9.553(3)	13.104(3)	14.480(5)	17.407(3)	13.726(14)	17.873(8)
c (Å)	17.646(7)	14.768(4)	27.895(6)	16.511(5)	13.333(6)	16.783(6)	17.546(4)	17.727(17)	14.084(5)
α (°)	90	90	90	90	81.75(3)	64.56(2)	113.16(3)	105.32(4)	90
β (°)	90	99.04(2)	90	90	65.25(3)	88.39(3)	102.55(3)	99.37(3)	91.72(3)
γ (°)	90	90	90	90	80.78(3)	87.16(3)	94.97(3)	110.92(6)	90
U (Å^3)	2456.5(18)	2497.7(14)	7466(3)	3523.2(19)	2445.4(17)	2510.8(14)	2399.1	2122(4)	2445.4(17)
Space group	$P2_12_12_1$	$P2_1/c$	$Pbca$	$Pna2_1$	$P1$	$P1$	$P1$	$P1$	$P2_1/n$
Z	4	4	8	4	2	2	4	2	4
D_{calc} (g cm^{-3})	3.735	3.473	2.827	2.787	3.170	2.247	3.577	2.806	3.542
Crystal size (mm)	0.28 × 0.20 × 0.05	0.20 × 0.18 × 0.03	0.15 × 0.15 × 0.10	0.40 × 0.16 × 0.02	0.13 × 0.10 × 0.07	0.32 × 0.30 × 0.24	0.22 × 0.20 × 0.18	0.36 × 0.29 × 0.25	0.44 × 0.18 × 0.16
Crystal habit	plate	plate	block	plate	block	block	block	block	needle
F(000)	2400	2296	5668	2664	2288	1572	2264	1606	2288
Radiation	Mo Kα	Mo Kα	Mo Kα	Mo Kα	Mo Kα	Mo Kα	Mo Kα	Mo Kα	Mo Kα
Wavelength (Å)	0.71073	0.71073	0.71073	0.71073	0.71073	0.71073	0.71073	0.71073	0.71073
μ (mm^{-1})	25.827	20.929	17.092	14.897	20.471	10.269	21.787	15.882	21.376
Transmission	0.052–0.358	0.155–0.672	0.1836–0.2798	0.0660–0.7549	0.1761–0.3283	0.1426–0.2562	0.379–0.875	0.146–0.747	0.065–1.000
Temperature (K)	293(2)	293(2)	290(2)	290(2)	290(2)	290(2)	293(2)	293(2)	293(2)
Diffractometer	Siemens R3mV	Siemens R3mV	Siemens R3mV	Siemens R3mV	Siemens R3mV	Siemens R3mV	Siemens R3mV	Stoe-Siemens	Siemens R3mV
Scan type	$\omega-2\theta$	$\omega-2\theta$	$\omega-2\theta$	$\omega-2\theta$	$\omega-2\theta$	$\omega-2\theta$	$\omega-2\theta$	$\omega-\theta$	$\omega-2\theta$
Data collection range (°)	$5.4<2\theta<42.08$	$7.16<2\theta<45.10$	$7.02<2\theta<45.08$	$5.12<2\theta<45.08$	$5.12<2\theta<45.08$	$5.0<2\theta<50.0$	$7.06<2\theta<45.1$	$7.04<2\theta<50.12$	$7.36<2\theta<45.08$
Index ranges	$-11\le h\le 11$, $0\le k\le 11$, $-3\le l\le 17$	$0\le h\le 12$, $0\le k\le 16$, $-15\le l\le 15$	$0\le h\le 13$, $0\le k\le 22$, $-4\le l\le 30$	$-24\le h\le 24$, $-10\le k\le 10$, $-17\le l\le 17$	$-1\le h\le 13$, $-13\le k\le 14$, $-13\le l\le 14$	$-12\le h\le 12$, $-14\le k\le 15$, $-3\le l\le 18$	$0\le h\le 9$, $-18\le k\le 18$, $-18\le l\le 18$	$-12\le h\le 12$, $-16\le k\le 15$, $-11\le l\le 21$	$0\le h\le 10$, $0\le k\le 19$, $-15\le l\le 15$
Reflections measured	2993	3512	5058	4922	5458	7081	6981	7577	3417
Independent reflections	2645 (R_{int} = 0.0536)	3213 (R_{int} = 0.0262)	4884 (R_{int} = 0.013)	4562 (R_{int} = 0.038)	5011 (R_{int} = 0.025)	7081 (R_{int} = 0.0093)	6288 (R_{int} = 0.038)	7453 (R_{int} = 0.065)	3099 (R_{int} = 0.038)
Parameters, restraints	174, 0	174, 0	239, 5	227, 0	496, 0	631, 0	469,0	527, 65	335,0
wR (all data)	0.2079	0.1878	0.1563	0.1189	0.1485	0.063	0.1185	0.121	0.140
$R_1[I>2\sigma(I)]$	0.071	0.0663	0.0788	0.0519	0.0542	0.035	0.044	0.045	0.045
Goodness-of-fit	1.030	1.048	1.019	1.042	1.020	0.810	1.089	1.093	1.058
Maximum shift σ	0.000	0.000	0.001	0.000	0.000	0.006	0.001	−0.003	0.001
Extinction coefficient	0.0030								0.0041
Peak, hole (e Å^{-3})	2.522, −2.230	3.133, −2.909	2.234, −1.826	1.770, −1.905	1.998, −1.949	0.96, −0.87	1.877, −2.123	2.848, −3.058	1.704, −2.175
Absolute structure parameter	−0.11(9)			0.00(2)					

reflux for 30 min, the solvent evaporated and the residue chromatographed using CH_2Cl_2:hexane as eluent, but no products could be isolated. The same method was applied to $P(OMe)_3$ (5 mg, 0.054 mmol) and PPh_2Me (10 mg, 0.050 mmol) with the same result.

3.2. X-ray crystallography

Suitable single crystals of the clusters **5**, **7**, **11**, **12**, **13**, **15**, **18**, **20** and **21** were glued on glass fibres with epoxy resin, and the assembly mounted on a goniometer head. This was transferred to a Siemens R3mV diffractometer or a Stoe-Siemens four-circle diffractometer (for **20**) and data was measured using graphite monochromated Mo Kα radiation ($\lambda = 0.71073$ Å). In each case a semi-empirical absorption correction based on Ψ-scans (EMPABS) was applied along with Lorentz and polarization corrections. Details of crystal data, data collection parameters, and structure and refinement parameters are presented in Table 11. All the structures were solved by direct methods (SHELXS-86 [32]) and subjected to full-matrix least-squares refinement on F^2 (SHELXL-97 [33]) except for **15** that was refined on F (SHELXL-93 [34]). In each structure the heaviest atoms including Os, Ru, Au, P, Cl and N, when present, were refined anisotropically; in structures **13**, **15**, **18**, **20** and **21**, the C and O atoms were also refined anisotropically; in the other structures they were refined with individual isotropic displacement parameters. Hydrogen atoms were included using rigid methyl groups or a riding model. Hydride ligands were placed in the positions generated by the HYDEX programme [14] and included in the model but were not themselves refined. In structures **11** and **20** one quarter and one half, respectively, of a disordered dichloromethane molecule was located in the crystal lattice; each of these molecules was refined with the appropriate partial occupancies, and with restraints to maintain a reasonable model geometry. In the final cycles of refinement a weighting scheme that afforded a relatively flat analysis of variance was introduced, and refinement continued until convergence was reached.

4. Supplementary material

Crystallographic data (excluding structure factors) has been deposited with the Cambridge Crystallographic Data Centre under the CCDC Nos. 188131–188139. Copies may be obtained without charge from The Director, CCDC, 12 Union Road, Cambridge, CB2 1EZ, UK (fax: +44-1223-336-033; e-mail: deposit@ccdc.cam.ac.uk or www: http://www.ccdc.cam.ac.uk).

Acknowledgements

The authors thank The Government of the Sultanate of Oman (M.R.A.A), The Overseas Research Students Awards (M.R.A.A.), The Cambridge Thai Trust (R.B.), the E.P.S.R.C (C.C., G.P.S.) and the Cambridge Crystallographic Data Centre (G.P.S.) for funding, the EU for a Human Capital and Mobility Grant (M.C.R. de A.) and Johnson Matthey PLC for the generous loan of Os and Ru salts. We are grateful to the University of Bath for a University Studentship (C.L.D.).

References

[1] (a) J. Lewis, P.R. Raithby, in: P. Braunstein, L.A. Oro, P.R. Raithby (Eds.), Metal Clusters in Chemistry, vol. 1, Wiley-VCH, Weinhein, 1999, pp. 348–380;
(b) P.R. Raithby, Platinum Metals Rev. 42 (1998) 146;
(c) B.F.G. Johnson, Coord. Chem. Rev. 190–192 (1999) 1269;
(d) D. Braga, P.J. Dyson, F. Grepioni, B.F.G. Johnson, Chem. Rev. 94 (1994) 1585;
(e) H. Wadepohl, Angew. Chem., Int. Ed. Engl. 31 (1992) 247.
[2] A.T. Brooker, P.A. Jackson, B.F.G. Johnson, J. Lewis, P.R. Raithby, J. Chem. Soc., Dalton Trans. (1991) 707.
[3] J. Lewis, C.-K. Li, P.R. Raithby, W.-T. Wong, J. Chem. Soc., Dalton Trans. (1993) 999.
[4] J. Lewis, C.-K. Li, M.C. Ramirez de Arellano, P.R. Raithby, W.T. Wong, J. Chem. Soc., Dalton Trans. (1993), 1359.
[5] (a) J. Lewis, C.-K. Li, C.A. Morewood, M.C. Ramirez de Arellano, P.R. Raithby, W.-T. Wong, J. Chem. Soc., Dalton Trans. (1994) 2159.;
(b) A.J. Amoroso, B.F.G. Johnson, J. Lewis, C.-K. Li, C.A. Morewood, P.R. Raithby, M.D. Vargas, W.-T. Wong, J. Clust. Sci. 6 (1995) 163.
[6] J. Lewis, C.A. Morewood, P.R. Raithby, M.C. Ramirez de Arellano, J. Chem. Soc., Dalton Trans. (1996) 4509.
[7] J. Lewis, C.A. Morewood, P.R. Raithby, M.C. Ramirez de Arellano, J. Chem. Soc., Dalton Trans. (1997) 3335.
[8] R. Buntem, J. Lewis, C.A. Morewood, P.R. Raithby, M.C. Ramirez de Arellano, G.P. Shields, J. Chem. Soc., Dalton Trans. (1998) 1091.
[9] N.L. Cromhout, J.F. Gallagher, J. Lewis, P.R. Raithby, Inorg. Chem. Commun. 2 (1999) 389.
[10] Z. Akhter, J.F. Gallagher, J. Lewis, P.R. Raithby, G.P. Shields, J. Organomet. Chem. 596 (2000) 204.
[11] R. Buntem, J.F. Gallagher, J. Lewis, P.R. Raithby, M.-A. Rennie, G.P. Shields, J. Chem. Soc., Dalton Trans. (2000) 4297.
[12] P.R. Raithby, G.P. Shields, Polyhedron 17 (1998) 2829.
[13] M.R.A. Al-Mandhary, J. Lewis, P.R. Raithby, J. Organomet. Chem. 530 (1997) 247.
[14] A.G. Orpen, J. Chem. Soc., Dalton Trans. (1980) 2509.
[15] G.R. John, B.F.G. Johnson, J. Lewis, W.J.H. Nelson, M. McPartlin, J. Organomet. Chem. 171 (1979) C14.
[16] D.-Y. Jan, L.-Y. Hsu, W.-L. Hsu, S.G. Shore, Organometallics 6 (1987) 274.
[17] W. Clegg, N. Feeder, A.M. Martin Castro, S. Nahar, P.R. Raithby, G.P. Shields, S. Teat, J. Organomet. Chem. 573 (1999) 237–246.
[18] B.F.G. Johnson, R. Khattar, J. Lewis, P.R. Raithby, J. Chem. Soc., Dalton Trans. (1989) 1421.
[19] G.R. Steinmetz, A.D. Harley, G.L. Geoffroy, Inorg. Chem. 19 (1980) 2895.

[20] W.K. Leong, F.W.B. Einstein, R.K. Pomeroy, Acta. Crystallogr., C 53 (1997) 24.
[21] B.F.G. Johnson, J. Lewis, P.R. Raithby, K. Wong, K.D. Rouse, J. Chem. Soc., Dalton Trans. (1980) 1248.
[22] M.Y. Darensbourg, in: S.J. Lippard (Ed.), Prog. Inorg. Chem. 33 (1985) 239.
[23] P.A. Dawson, B.F.G. Johnson, J. Lewis, D.A. Kaner, P.R. Raithby, J. Chem. Soc., Chem. Comm. (1980) 961.
[24] G.A. Foulds, B.F.G. Johnson, J. Lewis, R.M. Sorrell, J. Chem. Soc., Dalton Trans. (1986) 2515.
[25] Y. Hung, W.J. Keng, H. Taube, Inorg. Chem. 20 (1981) 457.
[26] M.A. Bennett, K. Smith, J. Chem. Soc., Dalton Trans. (1974) 233.
[27] S. Stahl, H. Werner, Organometallics 9 (1990) 1987.
[28] A.M. Mueting, B.D. Alexander, P.D Boyle, A.L. Casalnuovo, L.N. Ito, B.J. Johnson, L.H. Pignolet, Inorg. Synth. 29 (1992) 279.
[29] C. Cathey, J. Lewis, P.R. Raithby, M.C. Ramirez de Arellano, J. Chem. Soc., Dalton Trans. (1994) 3331.
[30] B.F.G. Johnson, J. Lewis, P.A. Kitty, J. Chem. Soc. A (1968) 2859.
[31] T.P. Gill, K.R. Mann, Organometallics 1 (1982) 485.
[32] G.M. Sheldrick, SHELXS-86, A Program for Crystal Structure Solution, University of Göttingen, Göttingen, Germany, 1986.
[33] G.M. Sheldrick, SHELXS-97, A Program for Crystal Structure Refinement, University of Göttingen, Göttingen, Germany, 1997.
[34] G.M. Sheldrick, SHELXS-93, A Program for Crystal Structure Refinement, University of Göttingen, Göttingen, Germany, 1993.